Refractive Indices Dispersion and Order of Lyotropic Liquid Crystal Polymers

Hedi Mattoussi,* Mohan Srinivasarao,† Philip G. Kaatz, and Guy C. Berry

Department of Chemistry, Carnegie Mellon University, 4400 Fifth Avenue, Pittsburgh, Pennsylvania 15213

Received July 2, 1991

ABSTRACT: Refractive index measurements of polymer liquid crystals in the nematic phase are described. The technique used, applicable for any birefringent uniaxial medium, makes use of the birefringence to generate interference between the extraordinary and ordinary waves created after an incident plane polarized wave enters the crystal. The procedures are used to measure the ordinary and extraordinary refractive indices n_o and n_e, respectively, of nematic solutions of the rodlike poly(*p*-phenylenebenzobisthiazole) (PBT) for wavelengths from the visible to near-infrared radiations. The measured birefringence is high, e.g., $|n_e - n_o|$ varies from 0.05 to 0.09 at 632.8 nm for polymer concentrations from 4×10^{-2} to 10×10^{-2} (g/cm^3). The birefringence is highly dispersive, and the dispersion is anisotropic: n_e has a more pronounced dispersion than n_o. The dispersion of the refractive indices (and consequently the birefringence) is correlated to the dichroism of these ordered media, as well as to the nonlinear optic properties subsequently achieved on these materials. The birefringence and its dependence on solute concentrations are discussed, with implications on the order parameter of these nematic solutions.

Introduction

The optical characterization of uniaxial, and nematic liquid, crystals requires the measurements of two refractive indices, the ordinary n_o and extraordinary n_e, defined, respectively, for plane waves traveling in the medium with polarization perpendicular or parallel to the optic axis of the system. Conventional thermotropic low molecular weight (lmw) and polymeric nematic liquid crystals have, in general, positive birefringence: $n_e - n_o > 0$, as opposed, for example, to discotic liquid crystals.[1-4] On the one hand, measurements of the birefringence $n_e - n_o$ of uniaxial lmw or polymeric liquid crystal media may be correlated to the order in these systems.[1-4] On the other hand, accurate measurements of the refractive indices n_e, n_o, and n_{iso} (isotropic) and their dispersion are used to analyze harmonic generation signals and the coupling between orientation and nonlinear optical (NLO) properties of such media.[5]

Poly(*p*-phenylenebenzobisthiazole) (PBT) is known to be rodlike.[6-8] Its solutions exhibit an isotropic to nematic transition if the rod concentration exceeds a temperature-dependent critical value c^*. This value is directly related to the aspect ratio L/D of the chain, where L and D designate the length and diameter of the rod, respectively.[9-12] Such media are known to have a moderate to high order parameter, $S > 0.7$ for instance.[13-16]

Because of its conjugated backbone, the nonlinear optical (NLO) properties of PBT are of great interest.[17] Studying such properties in the nematic phase is promising because of the high order of such solutions. As dissolution of this compound in strong acids is accompanied by protonation of the chain,[6-8,18] the NLO properties of PBT in solution will differ from those of the undiluted polymer. Measurement of the nonlinear optical susceptibilities $\chi^{(i)}$ ($i = 2$ and 3), using a common technique, optical harmonic generation, requires accurate knowledge of the refractive index n of the medium and its dispersion $n = n(\omega \text{ or } \lambda)$.[19-21] The dispersion must be known over a wide range of wavelengths, from UV-visible to near-infrared, for second and third harmonic generation (SHG and THG) techniques.

† Present address: Polymer Science and Engineering Department, University of Massachusetts, Amherst, MA 01003.

In this contribution, we present refractive index measurements of nematic PBT solutions for several wavelengths: 500 nm < λ < 2000 nm. Two related methods have been used, involving transmission of polarized light: (1) rotation of a plane parallel sample and (2) conoscopic microscopy. The second method has been applied only for visible wavelengths. In the first section, analysis of the methods is given, followed by a description of the experimental arrangements. Then a brief description of the materials, the solutions, and the nematic monodomain preparation is given. In the last section, the discussion involves correlation between the birefringence and the order parameter in these nematic solutions, the dispersion of the refractive indices and its relation to the dichroism of these ordered media, and also some implications on NLO properties of nematic PBT solutions.

Experimental Section

Theoretical Background. Use of the medium birefringence to generate interference of light between the extraordinary and ordinary waves propagating in a crystal is a known procedure for optical characterization and identification of uniaxial materials. A plane light wave incident on a uniaxial crystal with its polarization at some angle to the optic axis of the medium may be decomposed into two secondary waves, traveling with speeds $v'' = c/n''$ (extraordinary) and $v' = c/n'$ (ordinary), where n'' and n' are the extraordinary and ordinary refractive indices for the waves traveling in the crystal at an average direction eventually different from the principal axis of the medium, and c is the speed of light in vacuum. When these waves recombine and interfere at the exit, they have a light path difference δ (since $n'' \neq n'$).[22-24] A polarizer (P) may be used to define the incident polarization and an analyzer (A) to select the outgoing one, with an angle ψ between P and A. Let ϕ be the angle between the optic axis and the polarizer (or the incident polarization). A simple case used in the two methods discussed below has the optic axis n in the plane of the sample, and $\phi = \pi/4$, as shown in Figure 1a. The transmitted intensity I is then given by[22-24]

$$I = I_0[\cos^2 \psi - \sin 2\phi \sin 2(\phi - \psi) \sin^2 (\pi\delta/\lambda)] \quad (1)$$

where I_0 is the maximum possible transmission (I_0 depends on the transmission and reflection coefficients), and λ is the incident wavelength.[22-24] The oscillation of I with δ is enhanced by setting

0024-9297/92/2225-2860$03.00/0

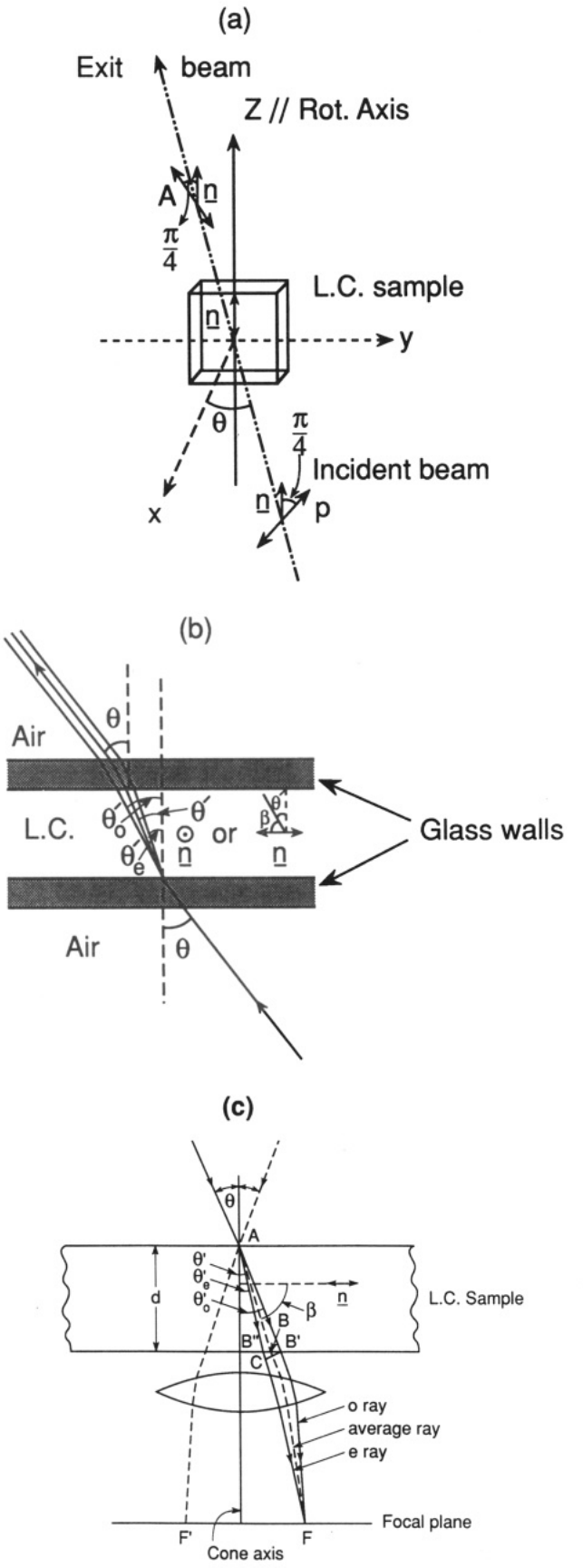

Figure 1. Schematical description of the sample and the polarization configuration for the interference process: (a) Geometry 1 ($\phi = \pi/4$) in the first method; a perspective view is given. (b) Light path(s), ordinary and extraordinary, in the crystal with the corresponding refraction angles θ_e' and θ_o'. (c) Schematical diagram for the diverging beam with different waves in the crystal for the second method; $\underline{n}$ is kept within the plane and normal to the cone axis.

$\psi = \pi/2$ and $\phi = \pi/4$ (or $-\pi/4$) (see Figure 1) so that

$$I = I_0 \sin^2 [\pi\delta/\lambda] \tag{2}$$

Because of the anisotropy of the medium, when an incident light beam enters the medium with an incident angle θ, the extraordinary and ordinary waves inside the crystal have refraction angles θ_e' and θ_o', respectively. Consequently, the waves travel with light path lengths, d_e' and d_o'. For the conditions described in Figure 1 (planar geometry), the optical path difference δ is given by[22-24]

$$\delta = d_e'(n'' - n_G \sin\theta \sin\theta_e') - d_o'(n' - n_G \sin\theta \sin\theta_o') \tag{3}$$

with

$$d_e' = \frac{d}{\cos\theta_e'} \quad \text{and} \quad d_o' = \frac{d}{\cos\theta_o'} \tag{4}$$

where d is the physical thickness of the sample, n_G is the glass (cell wall) refractive index, and θ_e' and θ_o' are related to θ through Snell's law:

$$n'' \sin\theta_e' = n' \sin\theta_o' = n_{air} \sin\theta \tag{5}$$

The refractive indices n'' and n' are angle dependent and are functions of the refractive indices n_e and n_o along the principal optical directions of the crystal; see below.[22-24]

The birefringence $|n_e - n_o|$ is always small compared to the refractive indices n_e and n_o ($|n_e - n_o| \ll n_e$ and n_o). This allows the use of the approximation $\theta_e' \simeq \theta_o' \simeq \theta'$ in eqs 3 and 4 and permits an analytical expression for $n'' - n'$.[22-24] Thus, for small $|n_e - n_o|$

$$d_e' \simeq d_o' \simeq d' = d/\cos\theta' \tag{6}$$

and

$$\delta \simeq \frac{d}{\cos\theta'}(n_e - n_o) \sin^2\beta \tag{7}$$

where using eq 5 for the angles θ and θ'

$$\langle n_s \rangle \sin\theta' = n_{air} \sin\theta \tag{8}$$

with β the angle between the direction of propagation of the light beam and the optic axis $\underline{n}$ (see Figure 1b,c). The angles θ' and β may be related trigonometrically.[22-24] For the cases with rays propagating in planes perpendicular or parallel to $\underline{n}$, $\beta = \pi/2$ and $\beta = \pi/2 - \theta'$, respectively (see below). These cases correspond to the configurations for which $\underline{n}$ is either normal to or within the plane of incidence, respectively. The latter is defined as the plane containing the light beam and the normal to the sample surface (s in Figure 2). The refractive index $\langle n_s \rangle$ for the average wave may be written as a function of β (hence θ') and ϕ to give

$$\frac{1}{\langle n_s(\phi,\beta)\rangle^2} = \left(\frac{\sin^2\phi}{n_o^2} + \cos^2\phi\left(\frac{\cos^2\beta}{n_o^2} + \frac{\sin^2\beta}{n_e^2}\right)\right) \tag{9}$$

The two cases introduced above, corresponding to $\beta = \pi/2$ ($\underline{n}$ normal to the plane of incidence) and $\beta = \pi/2 - \theta'$ ($\underline{n}$ within the plane of incidence), are of great interest and simplicity. Together with the conditions for the angle ϕ ($+\pi/4$ or $-\pi/4$), they will be referred to as geometry 1 for $\beta = \pi/2$ and $\phi = \pi/4$ and geometry 2 for $\beta = \pi/2 - \theta'$ and $\phi = -\pi/4$.

For geometry 1 ($\underline{n}$ normal to the plane of incidence), eq 7 becomes

$$\delta \simeq \left[\frac{d(n_e - n_o)}{\cos\theta'}\right] \tag{10}$$

where θ' is given by eq 8, with

$$\frac{1}{\langle n_s \rangle^2} = \frac{1}{2}\left(\frac{1}{n_e^2} + \frac{1}{n_o^2}\right) \tag{11}$$

The extraordinary and ordinary waves travel with refractive indices that are independent of the propagation angle θ', and the variation in δ reflects that of $d'(\theta')$ (eq 6). For geometry 2 ($\underline{n}$ parallel to plane of incidence), eq 7 becomes

$$\delta \simeq d(n_e - n_o) \cos\theta' \tag{12}$$

where θ' is given by eq 8, with

$$\frac{1}{\langle n_s(\theta')\rangle^2} = \frac{1}{2}\left(\frac{1}{n_o^2} + \frac{\cos^2\theta'}{n_e^2} + \frac{\sin^2\theta'}{n_o^2}\right) \quad (13)$$

The two waves travel in the crystal with refractive indices dependent on θ'. The difference between the refractive indices for geometries 1 and 2 (eqs 11 and 13, respectively) may be written as

$$\frac{\langle n_s\rangle^2}{\langle n_s(\theta')\rangle^2} \simeq 1 + \left(\frac{n_e - n_o}{n_e}\right)\sin^2\theta' \quad (14)$$

Since $|n_e - n_o| \ll n_{e,o}$, and $\sin\theta' < 1$, $\langle n_s(\theta')\rangle$ is always close to $\langle n_s\rangle$. For example, the relative difference in eq 14 is about 10% for a birefringence of 0.2, $n_e \simeq 1.5$ and at an angle $\theta' \simeq \pi/2$; it is smaller for lower angles. The corresponding difference for the refractive indices $[\langle n_s(\theta')\rangle - \langle n_s\rangle]/\langle n_s(\theta')\rangle$ is about 5%.

Two additional assumptions lead to a simple analytical approximation for δ: when the inequalities $|n_e - n_o| \ll n_o$ and n_e hold, $\langle n_s\rangle$ can be approximated by the refractive index $\bar{n}$ of the equivalent isotropic medium, defined as

$$\bar{n} = \frac{n_e + 2n_o}{3} \quad (15)$$

This approximation is reasonable when $|n_e - n_o|$ is small, e.g., for geometry 1:

$$\frac{\langle n_s\rangle^2}{\bar{n}^2} \simeq 1 + \frac{3}{5}\frac{|n_e - n_o|}{n_o} \quad (16)$$

Thus, $\langle n_s\rangle$ and $\bar{n}$ are close, even for a fairly large birefringence. For example, for the conditions described above for $\langle n_s\rangle$ and $\langle n_s(\theta')\rangle$ ($|n_e - n_o| \simeq 0.2$) the corresponding difference $[\langle n_s\rangle - \bar{n}]/\bar{n}$ is about 4%. Usually, the error committed by setting $\langle n_s\rangle$ and $\langle n_s(\theta')\rangle$ equal to $\bar{n}$ in the data analysis for the birefringence is very small; it is less than 10% for an average value $\langle n_s\rangle \simeq 1.5$ and at $\theta' = 90°$ (see eqs 17 and 18) and decreases for smaller angles.

A scan of the transmitted intensity as a function of the angle of incidence θ provides an oscillating function. The minima occur at values θ_i for which the corresponding light path difference δ_i is an integer multiple of λ:

$$\delta_i = m_i\lambda = d\left(1 - \left(\frac{\sin\theta_i}{\langle n_s\rangle}\right)^2\right)^{-1/2}|n_e - n_o|; \quad \text{geometry 1} \quad (17)$$

and

$$\delta_i = m'_i\lambda = d\left(1 - \left(\frac{\sin\theta_i}{\langle n_s(\theta_i)\rangle}\right)^2\right)^{1/2}|n_e - n_o|; \quad \text{geometry 2} \quad (18)$$

Experimentally, if d is known, either geometry can be used to determine the birefringence $|n_e - n_o|$, with $\langle n_s\rangle$ or $\langle n_s(\theta'_i)\rangle$ replaced by $\bar{n}$. However, a fit for the minima in the intensity curve I vs θ_i using the full expressions for $\langle n_s\rangle$ (or $\langle n_s(\theta')\rangle$) is required if values of the individual refractive indices are needed (see below).

In the following, two methods are described to vary the propagation angle θ' (hence δ), with subsequent analysis of the transmitted intensity, to estimate the birefringence or/and the refractive indices of the material. More precisely, analysis of the intensity, using approximate solutions for δ, including the replacement of $\langle n_s\rangle$ by $\bar{n}$, provides an estimate of $|n_e - n_o|$, whereas use of the full expressions can lead to an estimate of both n_e and n_o.

Method 1: Rotation of a Plane Parallel Slab. In this method, the variation of the phase difference is monitored as the path length in the crystal is varied by rotation of the sample with respect to the incident beam. The mean-field director $\underline{n}$ is always in the plane of the sample. The axis of rotation is kept normal to the plane of incidence (Figure 2). Geometry 1 corresponds to the conditions with the axis of rotation and the nematic director parallel, whereas geometry 2 corresponds to the case where they are perpendicular (Figures 1a and 2a). The optical path difference δ is given by eq 10 or eq 12, and $\langle n_s\rangle$ is given by eq 11 or eq 13, for the two cases, respectively. Rotation of the sample is accompanied by variation of β (hence θ') for geometry 2, but not for geometry 1.

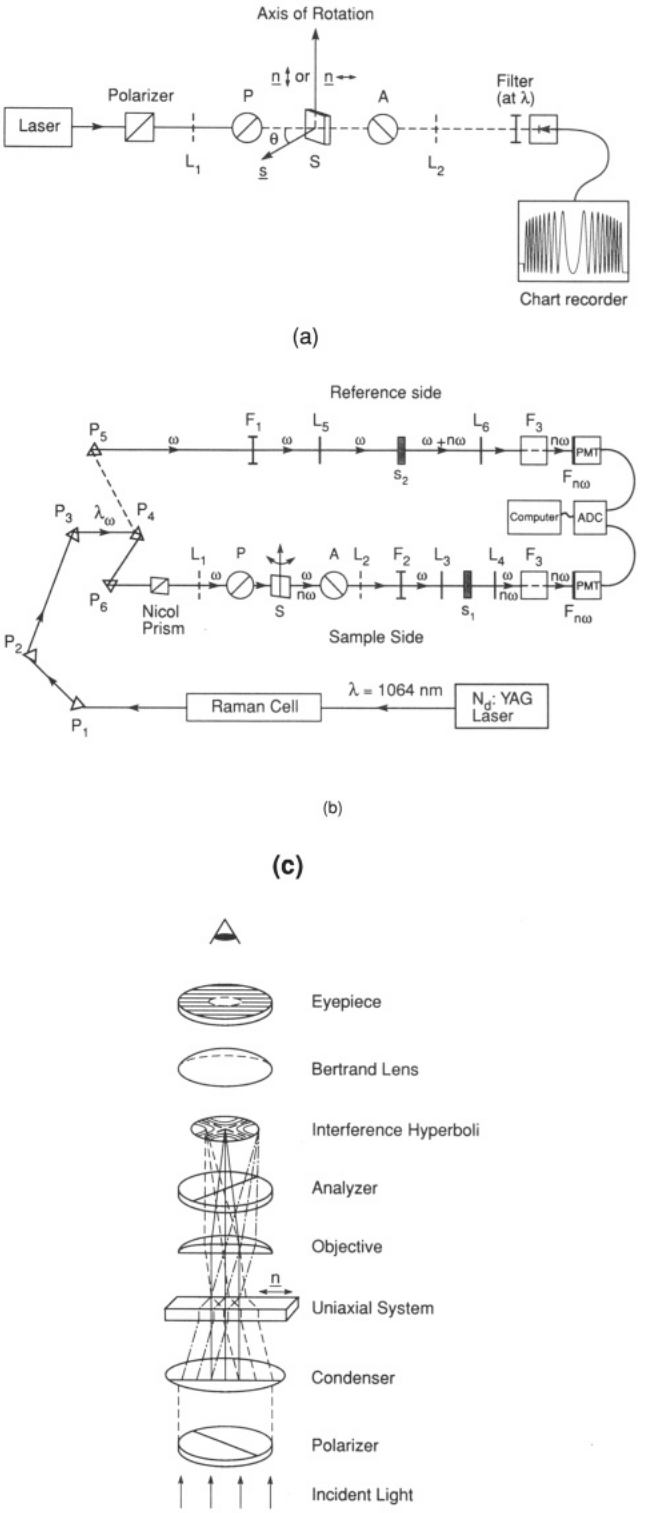

Figure 2. Experimental arrangement for the rotation of a plane parallel sample and conoscopic methods: (a) Visible radiation; $\underline{n}$ is always within the sample plane. (b) Harmonic generation apparatus for the incident IR radiation. Weakly converging lenses L_1 and L_2 may help in reaching a better definition of the light beam in the sample, and therefore for θ. (c) Schematical diagram for the conoscopy mode.

In practice, we proceed as follows: An estimate of $|n_e - n_o|$ is deduced from an experiment using geometry 1, together with the assumption $\langle n_s\rangle = \bar{n}$. The latter is estimated from the refractive index of the solvent and the increment $(\partial n/\partial c)$ for PBT solutions.[6,7] This $|n_e - n_o|$ is then used to fit the data for the same geometry, using eqs 10 and 11 for δ_i and $\langle n_s\rangle$, respectively, to

obtain both n_e and n_o. The latter values may be checked by fitting the experimental data for geometry 2 to the full expressions for δ_i and $\langle n_s(\theta_i)\rangle$ (eqs 12 and 13). The values taken for n_e and n_o are those which provide the best fit for the experimental data for both geometries. Limiting the numerical fit to the experimental data for geometry 1, which is simpler because $\langle n_s\rangle$ is independent of θ', will usually provide values for the individual refractive indices. However, it is useful to apply both geometries when initial estimates for n_e and n_o are poorly defined.

Method 2: Conoscopy. In the conoscopic mode, a crystal is examined in highly convergent light between crossed polars.[22-24] Because of the convergent nature of the beam, the optical properties of the crystal are observed simultaneously at many propagation angles in the medium. A schematical description of this method is shown in Figure 1c. The path difference δ is a function of the angle made by this ray on the cone of light. Consequently, when the transmitted beam is brought to interference in the focal plane of a lens, every point in this plane is associated with a direction of parallel rays entering and leaving the crystal (a finite angle on the cone).

For a planar nematic monodomain ($\underline{n}$ laying in the sample plane), the parameter δ is expressed as a function of the angles that a ray on the cone of light forms with respect to the cone axis and to the optic axis $\underline{n}$, θ' and β, respectively. Because the cone axis is taken normal to the sample surface, the angle of propagation of the ray on that cone is also the angle of refraction. For a small birefringence, δ is given by eq 7.[22-24] For details about how the interference figure is formed for such media, see, e.g., refs 23 and 24. We simply recall that, for a sample between crossed polars (P and A), with its optical axis at an angle $\pi/4$ with respect to P and A, the interference figure is a set of hyperbolic isochromatic fringes centered around the cone axis if $\underline{n}$ is orthogonal to the microscope optic axis.[22-24] The interference figure reflects the symmetry of the medium: point inversion and mirror reflection around $\underline{n}$. The set of fringes rotates with $\underline{n}$ as the latter is rotated within the the sample plane and disappears when $\underline{n}$ is parallel to either P or A.[25] Scanning the corresponding values of θ' on the cone of light and within the focal plane reveals oscillations of the intensity as predicted by eq 2. A simplification of the expression for δ (eq 7) arises for all directions of propagation within planes corresponding to geometries 1 and 2 to give eqs 10 and 12, respectively. A more complex formulation is required if an arbitrary direction of propagation is chosen, and an extra dependence on β emerges.[25] In practice, the angle θ' is determined by referring to the numerical aperture of the lens, so that each point on the conoscopic figure can be related to an angle θ'. In principle, both geometries ($\beta = \pi/2$ and $\beta = \pi/2 - \theta'$) can be used to estimate the birefringence, given the sample thickness d and replacing $\langle n_s\rangle$ by $\bar{n}$. Only the first case, $\beta = \pi/2$, where δ and $\langle n_s\rangle$ are given by eqs 10 and 11, respectively, is used in the present study to provide values for the birefringence.

Experimental Arrangements. 1. Rotating Sample. The experimental setup is shown schematically in Figure 2. For the visible radiation, a cw laser (Spectra Physics) was used as the light source (Figure 2a). Two wavelengths were used: $\lambda = 514.5$ nm with an Ar ion laser and $\lambda = 632.8$ nm with a He–Ne laser. A Nicol prism (CVI Laser Corp.) was used to provide a polarized incident light beam. A rhomb rotator (Karl Lambrecht Inc.) was used as the polarizer (P), and a polarizing film was used as an analyzer (A), with an angular resolution of 0.1°. A silicon photodiode connected to a chart recorder was used to record the transmitted intensity.

For the infrared (IR) region, the light source was a pulsed Nd:YAG laser (Figure 2b). It provides an intense nanosecond pulse at $\lambda = 1064$ nm. A Raman cell was used as the source for the other IR wavelengths.[26] Pumped with the incident YAG signal, pulsed signals at $\lambda = 1542$ nm and $\lambda = 1907$ nm (Stokes components) were generated from methane and hydrogen gases, respectively. The pulse duration, the incident radiation wavelength, and the quantum efficiency of the photomultiplier caused a problem in detection. To circumvent these limitations, the IR beam exiting the crystal was used as a source to generate optical harmonic(s) on passage through a suitable material (component s_1 in Figure 2b).[19-21,26,27] The signal at 2ω or 3ω (for second and third harmonic generation processes) always falls within the UV–visible region and is therefore easy to detect. In addition to the polarizer and analyzer used for experiments with visible radiation, an IR band-pass filter (F_2 placed after the sample) is used to select the signal at ω after the sample, eliminating the harmonic signal generated from the sample, which also oscillates with θ, though with a different dependence on θ (i.e., Maker Fringes).[19-21] Two extra filters (F_3), a visible band pass and an interference filter, are needed to select the signal at 2ω (or 3ω) after the harmonic generation sources (Figures 2b). The signal at 2ω (3ω) is detected using a photomultiplier tube and then digitized through the use of an ADC system [CAMAC]. The sample signal is normalized by the signal for the reference to account for fluctuations in the pulsed source intensity (see Figure 2b). Since the harmonic signals are proportional to a power of the incident intensity, e.g., $I_{2\omega} \propto (I_\omega)^2$, and $I_{3\omega} \propto (I_\omega)^3$, these signals reproduce exactly the periodicity of I_ω on the rotation angle θ.[19-21] Consequently, the data analysis for the variation of the intensity with the angle of incidence θ is identical to that discussed above. The second harmonic process was found to provide sharper minima and consequently better angular resolution, because of the dependence on I_ω (I_ω^2 instead of I_ω^3).

2. Conoscopy. An optical microscope (Leitz) equipped with a set of polars placed before and after the sample is used in this method. The same arrangement is often used to examine liquid crystal samples.[12,28] However, an extra set of lenses is required for conoscopic use. A short focal lens is used before the sample to provide a converging light beam with a large cone angle (Numerical Aperture: $\sin\theta_{max} \simeq 0.6$). Another lens (Bertrand lens) is required to bring the interference figure to the plane of observation (Figure 2c). Experimentally, the distance between the two fringes is measured using a micrometer mounted on the microscope. This distance is converted to the corresponding angles on the cone, using the numerical aperture of the lens placed before the sample. Details on the experimental arrangement can be found in general review(s) on optical microscopy.[29-31] The spacing between the fringes could also be measured from a photographic picture or the screen of a videorecording of the interference figure, knowing the experimental conditions.

Materials and Sample Preparation. The polymer liquid crystal used for this present study is formed by solutions of poly(*p*-phenylenebenzobisthiazole) (PBT). The material was provided as solutions in poly(phosphoric acid) (PPA) by SRI International (Stanford, CA) through the courtesy of Dr. J. F. Wolfe. The synthesis procedures are described elsewhere.[6-12,18] The PPA solution was diluted in methanesulfonic acid (MSA), precipitated in methanol, thoroughly washed with water, freeze-dried, and stored in a dry atmosphere.

Freshly distilled MSA was used to prepare the solutions. Solution preparation was carried out under nitrogen atmosphere to avoid contamination by atmospheric moisture. The solutions were stirred (using a magnetic stirrer) for several days, until homogeneous media were formed. This process is slow because of the high viscosity of these solutions ($\eta > 1000$ P). We used PBT with weight-average molecular weight $M_W = 34\,000$, determined by light scattering measurements.[7,11] This corresponds to a weight-average rod length of 160 nm and an index of polymerization of 140. An aspect ratio of $L/D \simeq 300$ (where L stands for the rod length and D is the nominal diameter) provides a critical concentration for the isotropic to nematic transition of about $w \simeq 0.03$ wt ($c \simeq 4.44 \times 10^{-2}$ (g/cm^3)) in MSA solutions.[6-12]

Liquid crystal monodomains were obtained using flat cells of 200-, 300-, and 370-μm thickness with good optical quality ($\lambda/4$ surface flatness) provided by Hellma Cells, Inc. The same cell(s) and, consequently, the same samples were used for NLO harmonic generation measurements. Nematic monodomains were prepared as follows. The solution was extruded into the sample through a luer joint. Prealigned rods adsorb on the surface walls, and orientational order propagates through the bulk of the sample on subsequent annealing.[6-12] Nevertheless, this process is not always sufficient to provide a monodomain structure. Good quality monodomains, useful for optical purposes, are obtained by applying a strong magnetic field ($\mathbf{H} \simeq 4$ T) to freshly prepared samples for several hours, with $\mathbf{H}$ parallel to the sample walls and to the initial flow direction. The monodomains thus reached are stable indefinitely (provided they are kept dry). All measurements were done on monodomains which had been outside

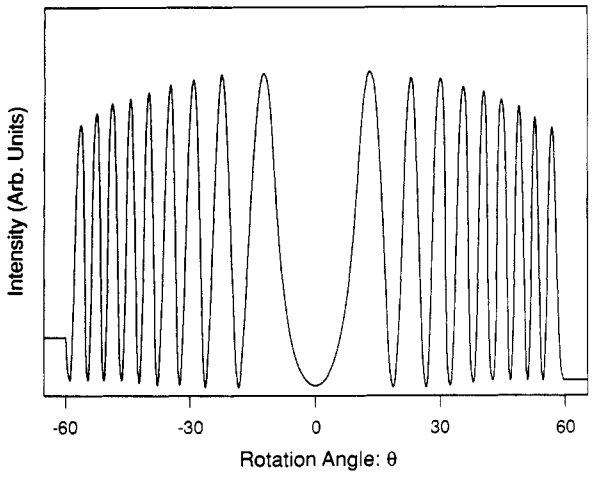

Figure 3. Transmitted intensity as function of the rotation angle θ for the visible radiation case: λ = 632.8 nm (He–Ne red line), d = 200 μm, $c = 7.15 \times 10^{-2}$ (g/cm^3).

the magnetic field for several hours. Consequently, no direct effects of the aligning field on the present data are expected, since the sample had previously reached equilibrium outside the field before the measurements were taken. The alignment quality of the planar sample subsequently obtained was checked by looking at the extinction properties of the transmitted white light between crossed polars: full extinction occurs when n is parallel to either analyzer (A) or polarizer (P), as is done for nematic lmw liquid crystals.[1-4] Another check was provided by the conoscopic figures obtained for these monodomains (Figure 6b). As outlined in the previous section for method 2, the point inversion and mirror reflection around n are observed. This was always compared against conoscopic figures given by a conventional uniaxial crystal (quartz) used as a reference (Figure 6). The quartz crystal is a flat slab of 4190-μm thickness, with its optical axis laying within the sample plane. It served for reference measurements for both methods used in the present study.

Results

A typical interference figure for a rotating plane parallel sample is given in Figure 3, showing the oscillatory function predicted by eq 2 for $I(\theta)$. The angles θ_j for the minima, as well as their number for a given rotation interval, depend on the geometry (n parallel or perpendicular to the rotation axis), the wavelength λ, the sample thickness d, and the medium birefringence. More oscillations occur for smaller λ, larger d, and/or larger $|n_e - n_o|$. Similar plots for the intensity $I_{2\omega}$ (and $I_{3\omega}$) vs θ for infrared radiation (pulsed source) are shown in Figures 4 and 5. Each point on the graph corresponds to a value of the angle θ and to an intensity averaged over 10 pulses. Parts a–c of Figure 4 refer to the PBT monodomain, whereas parts a and b of Figure 5 correspond to the quartz crystal. As mentioned above, better resolution for the minima location is obtained when second harmonic generation (SHG) is used (compare Figures 4a,b and 5a with Figures 4c and 5b). However, a third harmonic generation process was needed for λ = 1907 nm, as $\lambda(2\omega)$ = 953.5 nm falls within the IR region and is, therefore, not detected by the photomultiplier used.

Conoscopic interference figures are shown in Figure 6 for a nematic planar monodomain (solution with $w \simeq$ 0.0483 (wt) or $c \simeq 7.15 \times 10^{-2}$ (g/cm^3)) together with the corresponding interference pattern for the quartz planar crystal, at the He–Ne red line (λ = 632.8 nm). We checked to ensure that the interference figure rotates with the mean-field director as the sample is rotated within its plane, P and A being fixed and crossed.[12,25] As expected, the fringe spacing is invariant to such an operation, whereas the contrast between the dark and bright fringes varies with

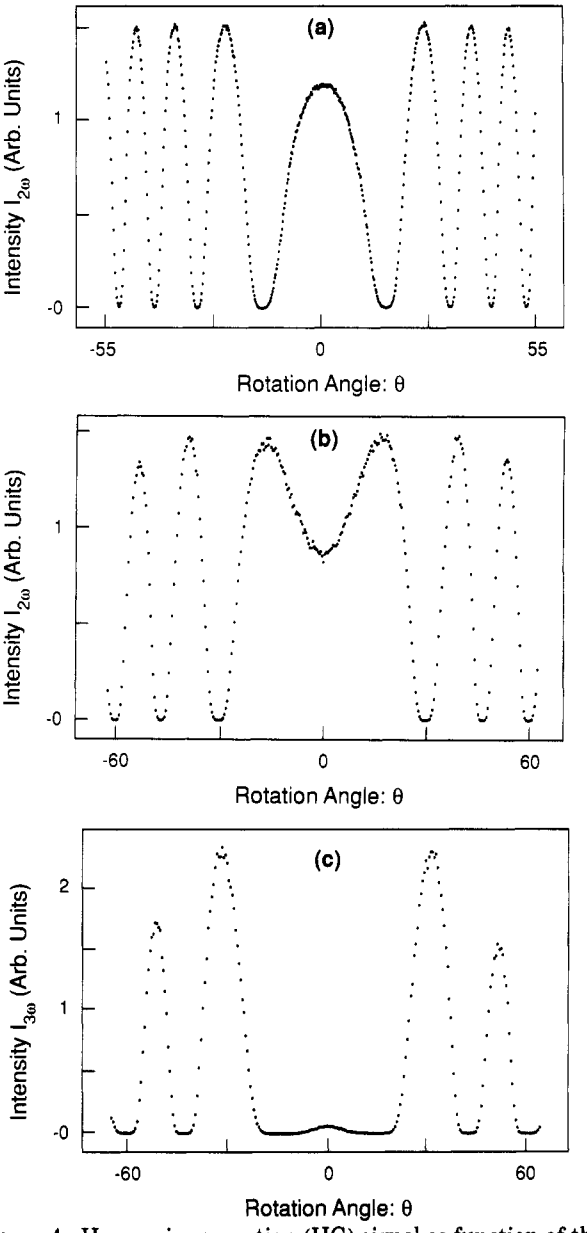

Figure 4. Harmonic generation (HG) signal as function of the rotation angle from the PBT monodomain ($c = 8.13 \times 10^{-2}$ and d = 370 μm): (a) SHG signal at λ_ω = 1064 μm. (b) SHG signal at λ_ω = 1542 nm. (c) THG signal at λ_ω = 1907 nm.

rotation of n with respect to its initial direction (n at 45° with respect to P) or when the angle between P and A is changed, keeping n fixed. The fringes disappear when n is parallel to either A or P (see the previous section). Values for the birefringence $|n_e - n_o|$, using the approximate expression for δ (eqs 10 and 12) and $\langle n_s \rangle = \bar{n}$ to fit the minima in I vs θ curves for geometries 1 and 2 (method 1), are reported in Table I for the different wavelengths used. We also report, in the same table, values for $|n_e - n_o|$ using method 2 and eq 10 (with $\langle n_s \rangle = \bar{n}$) for visible He–Ne radiation, λ = 632.8 nm. The corresponding values measured for the quartz slab using the same procedures are also given, together with those reported in the literature.[32] For the quartz reference slab, it is important to notice the agreement between the values of $|n_e - n_o|$ measured using method 1, with its two geometries, and those reported in the literature. In addition, the values deduced for a PBT monodomain using the approximate fit for each geometry are also in agreement for the two methods, showing the usefulness of the approximations made for the estimation of the birefringence. Nevertheless,

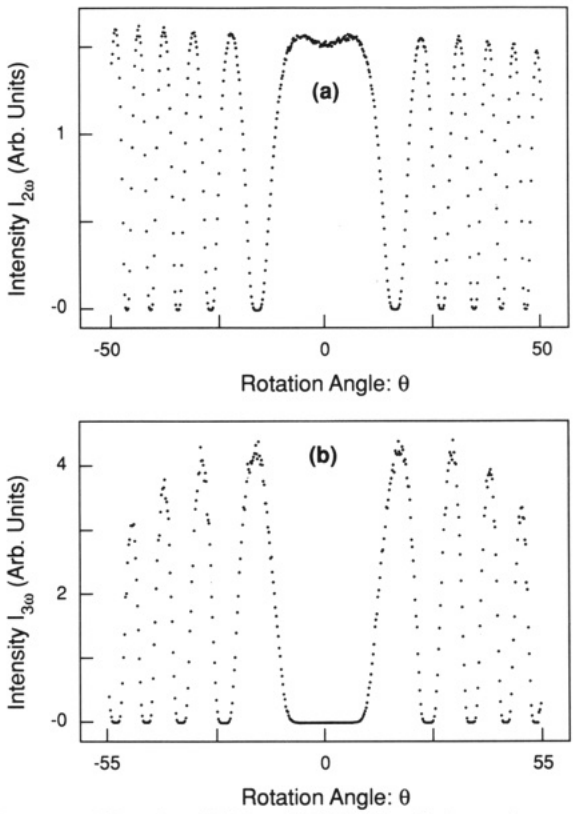

Figure 5. Plots for SHG and THG signals from the quartz reference (a) SHG at $\lambda = 1064$ nm and (b) THG at $\lambda = 1542$ nm. The minima for the THG pattern are broader than what is observed for the SHG case.

the values provided by geometry 2 (method 1), where $\langle n_s \rangle$ is angle-dependent (eq 13), are slightly larger than those obtained with geometry 1.

The use of the full expression for $\langle n_s \rangle$ (eq 11, geometry 1) in the data analysis (numerical fit) provides values for the individual refractive indices n_e and n_o and the corresponding $|n_e - n_o|$ as summarized in Table II. No numerical fit for geometry 2 where a more complex expression for $\langle n_s(\theta') \rangle$ is involved (eq 13) is presented. However, we checked that such a fit provided values for $n_{e,o}$ within 1–2% of those provided by geometry 1. The values for the birefringence $|n_e - n_o|$, deduced from the numerical fit, are in much better agreement with those provided by the "approximate" analysis for geometry 1: $|n_e - n_o|$ is within 1–3% of what has been deduced previously (approximate analysis in geometry 1) for all wavelengths.

Discussion

The birefringence shows pronounced dispersion for visible wavelengths: $|n_e - n_o|$ increases by a factor of about 2.5 when λ decreases from 1 to 0.5 μm, whereas its increase is less than 20% in the range $1 < \lambda < 2$ μm (see Figure 7). The dispersion of $|n_e - n_o|$ for the lower wavelengths is slightly more pronounced than reported for conventional liquid crystals (pure materials): $|n_e - n_o|$ increases by a factor of 2 for MBBA for λ in the visible spectrum, for instance.[33] However, the analysis of the variation of the individual refractive indices n_e and n_o shows that the dispersion is more pronounced for the extraordinary refractive index only at wavelengths in the visible spectrum (Figure 8). Isotropic solutions of PBT in MSA are known to have a modest absorption band centered around 436 nm, and their ordered nematic monodomains are dichroic, with an enhanced dichroism for smaller wavelengths in the visible spectrum.[12] For instance, the transmission

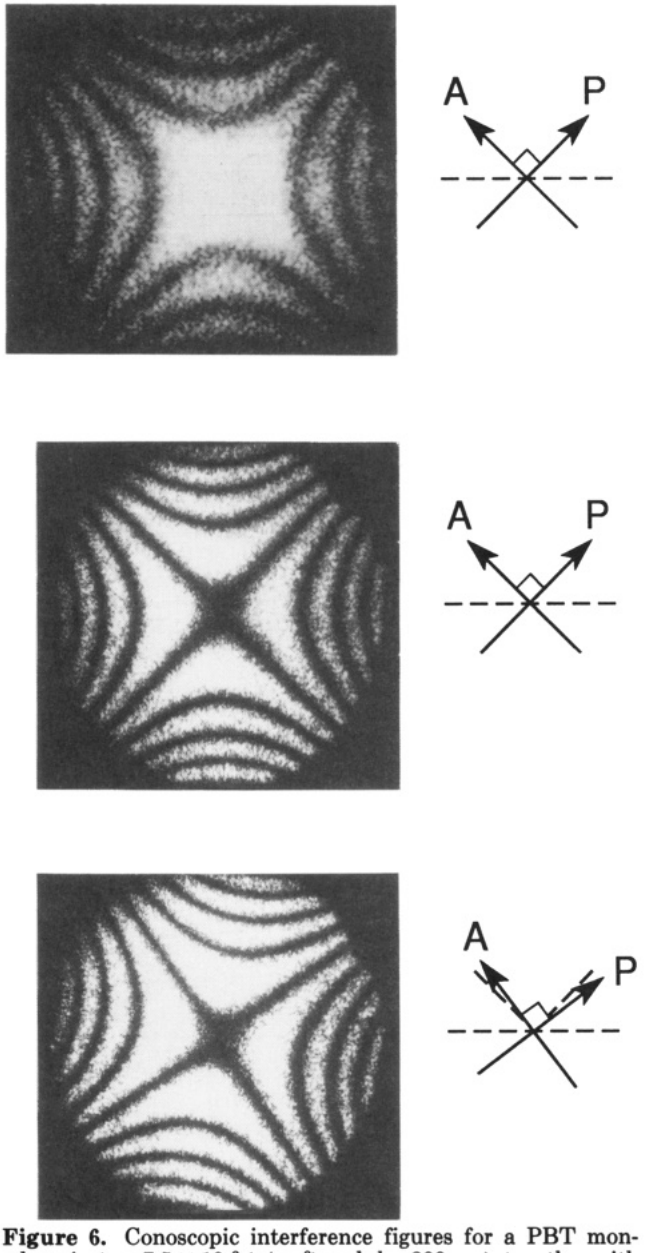

Figure 6. Conoscopic interference figures for a PBT monodomain ($c = 7.5 \times 10^{-2}$ (g/cm^3) and $d = 300$ μm), together with the quartz reference (top and middle figures, respectively); crossed polars and n at $\pi/4$ with respect to P and A. The bottom figure corresponds to a tilted crystal within its plane; the interference figure is slightly rotated within its plane.

coefficient of a plane polarized light is about 2 times larger for polarization normal to n ($\underline{E} \perp \underline{n}$) than the case where $\underline{E}$ and n are parallel ($\underline{E} \parallel \underline{n}$), at the green line ($\lambda = 514.5$ nm) and for a nematic monodomain of 300-μm thickness and a polymer concentration $w = 0.055$ wt.[12] Therefore, the strong dispersion of $|n_e - n_o|$ for small λ may be mainly attributed to the effects on n_e, and a meaningful discussion of the dispersion ought to consider each refractive index separately.

For many organic molecules, the dispersion may be represented by an empirical expression (similar to the Cauchy formula), based on a calculation using the Lorentz oscillator. For frequencies ν far from an absorption band centered around ν_m, this relation reduces to[23,24,34]

$$R = \frac{n^2 - 1}{n^2 + 2} \simeq \frac{K\nu_m^2}{\nu_m^2 - \nu^2} \tag{19}$$

where $K\nu_m^2$ is an average oscillator strength. The latter

Table I
Birefringence for PBT Monodomains and Quartz Crystal

	$\lvert n_e - n_o \rvert$						
	method 1: rotation of a plane parallel sample						
	geometry 1 ($n \parallel z$ axis)		geometry 2 ($n \perp z$ axis)		method 2: conoscopy		
wavelength λ, nm	PBT (d=370 μm), $c = 8.13 \times 10^{-2}$ g/cm^3	quartz (d=4190 μm)	PBT (d=370 μm), $c = 8.13 \times 10^{-2}$ g/cm^3	quartz (d=4190 μm)	PBT (d=300 μm), $c = 7.58 \times 10^{-2}$ g/cm^3	quartz (d=4190 μm)	quartz lit.[32]
514.5	0.125 ± 0.002		0.137 ± 0.002				0.009 24
632.8	0.0788 ± 0.005	0.0091	0.083 ± 0.002	0.0093	0.072	0.009	0.009 11
1064	0.0492 ± 0.0002	0.0087	0.051 ± 0.003	0.0088			0.008 78
1542	0.0452 ± 0.0005	0.0084		0.00857			0.008 49
1907	0.045 ● 0.001	0.0082					0.008 2

Table II
Values for the Refractive Indices n_e and n_o and the Birefringence $\lvert n_e - n_o \rvert$ Determined Using the Numerical Fit as Described in the Text

	PBT in MSA, $c \simeq 8.13 \times 10^{-2}$ g/cm^3			quartz crystal (d = 4190 μm)		
λ, nm	n_o	n_e	$\lvert n_e - n_o \rvert$	n_o	n_e	$\lvert n_e - n_o \rvert$
514.5	1.5270	1.6480	0.1210			
632.8	1.4990	1.5770	0.0780	1.543 30	1.552 44	0.009 14
1064	1.4389	1.4888	0.0499	1.534 30	1.543 04	0.008 74
1542	1.4340	1.4801	0.0461	1.528 60	1.537 08	0.008 48
1907	1.4294	1.4743	0.0449	1.520 8	1.529 02	0.008 22

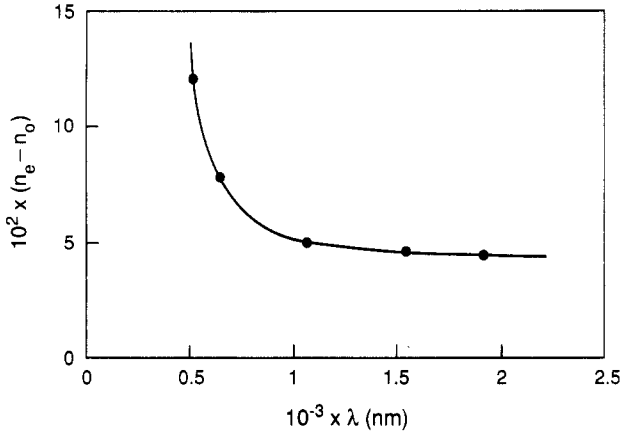

Figure 7. Plot for the birefringence $\lvert n_e - n_o \rvert$ vs λ. A monodomain with $c \simeq 8.13 \times 10^{-2}$ (g/cm^3) and a sample thickness d = 370 μm was used.

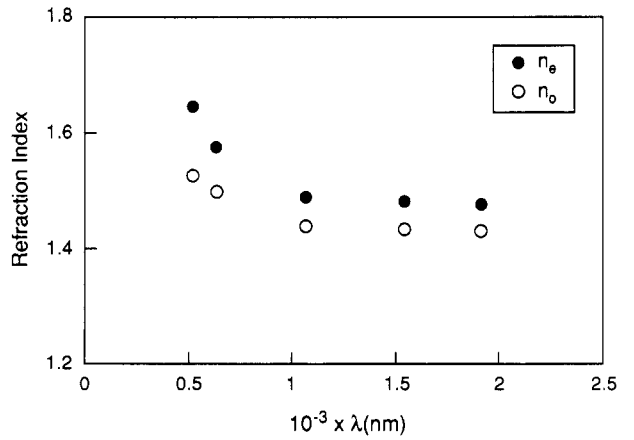

Figure 8. Plot for the absolute refractive indices vs λ. The top curve is for n_e, whereas the bottom curve is for n_o.

results from an integration over all contributing individual oscillators in the molecule and is related to the absorption coefficient of the medium. Equation 19 predicts a straight line for a fit of $1/R$ vs ν^2. Such a relation has been used fairly successfully to interpret the dispersion of the refractive index data for many dense systems and at wavelengths far from the absorption peak ν_m.[34] For uniaxial materials, eq 19 may be used for the refractive indices n_e and n_o, with constants ν_m and K for each. Plots for the experimental values for $1/R$ as a function of ν^2 are shown for both n_e and n_o in Figure 9. Agreement with eq 19 is observed for both cases over the range of wavelengths scanned, giving $\nu_m \simeq 12 \times 10^{14}$ s^{-1} (or $\lambda_m \simeq 250$ nm) for n_e, $\nu_m \simeq 15 \times 10^{14}$ s^{-1} (or $\lambda_m \simeq 200$ nm) for n_o, and K = 0.27 for both n_e and n_o. The emergence of two separate absorption frequencies, $(\nu_m)_e$ and $(\nu_m)_o$, in the UV region of the spectrum, suggests that PBT ordered solutions have two closeby spaced absorption lines at lower wavelengths. This may be reflected in the dichroism of these monodomains observed for visible radiation. The $K\nu_m^2$ values for n_e and n_o, which are associated with dichroism in the absorption properties for these monodomains in the UV, suggest a higher absorption coefficient for the ordinary case. By contrast, around the absorption maximum in the visible (436 nm) region the extraordinary case is more strongly absorbed, but with an extinction coefficient less than that in the UV. Apparently the latter dominates the dispersion of the refractive indices.

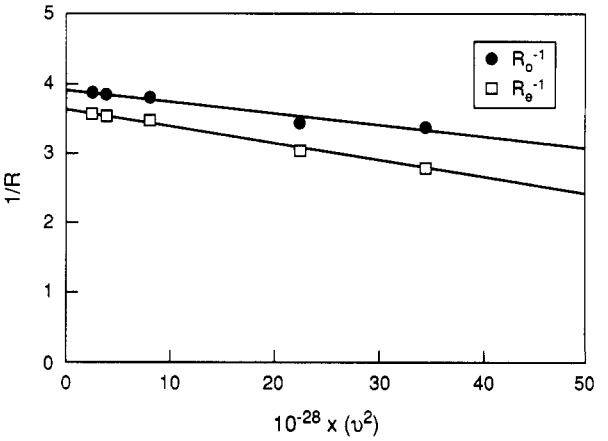

Figure 9. Plot of $1/R$ vs ν^2 for both refractive indices: ordinary and extraordinary.

The present dispersion data and their strong anisotropy have direct implication on the NLO data for these ordered solutions using third harmonic generation (THG) technique. An important parameter in such measurements, crucial for the signal analysis, is the coherence length, defined at normal incidence as[19-21]

$$l_c(\theta=0) = \frac{\lambda_\omega}{2m\lvert n_{3\omega} - n_\omega \rvert} \qquad (20)$$

where m is 2 or 3 for second or third harmonic generations, respectively. It characterizes the distance below which the interference of the harmonic signal is constructive. The dispersion is also involved in the estimation of the nonlinear optical coefficient: $\chi^{(m)}$, where the factor $[\chi^{(m)}/(n_{m\omega}^2 - n_\omega^2)]^2$ is the one actually extracted from the harmonic signal.[19-21] Use of the present data for the

Table III
Birefringence for Different Concentrations

10^2c, g/cm^3	$\lvert n_e - n_o \rvert$	method used
4.93	0.047	rotating sample, geometry 1
	0.046	conoscopy
6.30	0.059	conoscopy
7.15	0.0676	rotating sample, geometry 1
	0.067	conoscopy
7.58	0.078	conoscopy
8.13	0.0788	rotating sample, geometry 1
9.88	0.094	conoscopy

dispersion of both n_e and n_o in the analysis of THG data collected for ordered PBT solutions will be discussed in subsequent work.[35]

The order parameter S, defined as[1-4]

$$S = \left\langle \frac{3\cos^2 \Omega - 1}{2} \right\rangle \tag{21}$$

characterizes the "degree" of alignment of the rods in nematic media. Here Ω is the angle made by the rods with respect to the mean-field direction, and the broken brackets designate an ensemble average. In lyotropic media, such as PBT nematic solutions, S is mainly dependent on the solute concentration but also on the temperature. The order can be related to the optical properties of the medium and thus to the birefringence, $\lvert n_e - n_o \rvert$, as has been done for conventional low molecular weight liquid crystals.[1-4,36,37] Over the concentration range of interest here, this relation reads as

$$\lvert n_e - n_o \rvert \sim \lvert n_e - n_o \rvert_{MOL} S\Phi \tag{22}$$

where Φ is the solute volume fraction, and the "molecular birefringence" $\lvert n_e - n_o \rvert_{MOL}$ may be approximated by

$$\lvert n_e - n_o \rvert_{MOL} \simeq \frac{2\pi(n_{sol}^2 + 2)}{3n_{sol}} \left(\frac{N_A \rho \lvert \gamma_\parallel - \gamma_\perp \rvert}{M} \right) \tag{23}$$

with ρ the solvent density and $\gamma_\parallel - \gamma_\perp$ the difference between the principal molecular polarizabilities parallel and perpendicular to the rod axis, respectively. The parameter $\lvert n_e - n_o \rvert_{MOL}$ is equal to the measured birefringence for both S and Φ equal to 1. Equation 23 is based on the expression[35]

$$\frac{4}{3}\pi N \alpha_j = \frac{n_j^2 - 1}{\langle n^2 \rangle + 2}; \; j = e, o \tag{24}$$

for the extraordinary and ordinary components of the polarizability, with

$$\langle n^2 \rangle = \frac{n_e^2 + 2n_o^2}{3} \tag{25}$$

Values of the birefringence $\lvert n_e - n_o \rvert$ for $\lambda = 632.8$ nm, where absorption is small, are reported for a few concentrations in Table III. The corresponding plot is shown in Figure 10, and a linear curve results, for which

$$\lvert n_e - n_o \rvert = 1.46S(\Phi - 0.002); \quad \text{for } \Phi > 1.1\Phi^* \tag{26}$$

On the basis that S should not decrease with increasing Φ, the data in Figure 10 give S at Φ^* equal to $1 - 0.002/\Phi^*$, or 0.94, and $\lvert n_e - n_o \rvert_{MOL} = 1.46$.[6,7] By comparison, an analysis for $\lvert n_e - n_o \rvert_{MOL}$ for PBT in MSA based on $\lvert \gamma_\parallel - \gamma_\perp \rvert$ determined in dilute solution gives $\lvert n_e - n_o \rvert_{MOL} = 1.55$.[6,7,9,10,39]

The behavior in Figure 10 suggests that S is close to 0.94 over the entire range of concentration studied. This is particularly high since the smallest concentration studied is very close to the critical value ϕ^*, for the threshold of

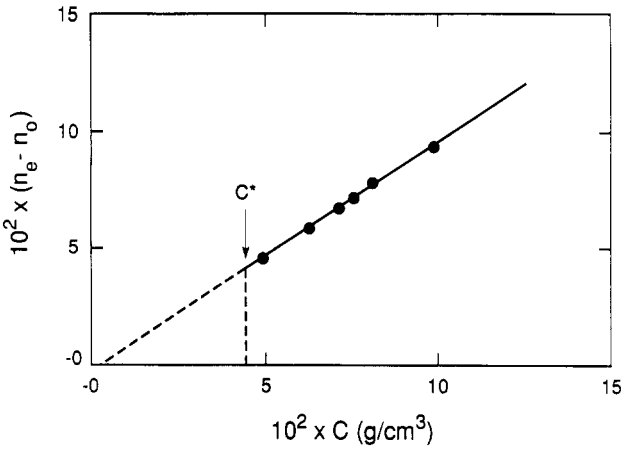

Figure 10. Plot for the birefringence $\lvert n_e - n_o \rvert$ as a function of the concentration c. The values of c scanned are within the range slightly above the critical concentration indicated by the arrow.

the isotropic to nematic transition, e.g., $\phi/\phi^* \simeq 1.1$. The result, S constant, over a fairly wide range of concentrations ($1 < (\phi/\phi^*) < 2.5$), is new. The order parameter has been found to depend on ϕ for other lyotropic media, and the value of S at ϕ slightly above ϕ^* is smaller than that reported here.[13-16] For example $S = 0.75$ was reported for aqueous TMV solutions with $\phi/\phi^* \simeq 1.05$, with S reaching 0.95 for $\phi/\phi^* = 1.5$, whereas a value of about 0.7 was reached for PBLG at $\phi/\phi^* \simeq 1.2$ and $S = 0.8$ for $\phi/\phi^* = 1.8$.[13-16] The charged, rodlike nature of PBT, and the high aspect ratio ($L/D \simeq 300$) may enhance the order in the solutions.[40,41]

The birefringence measured for PBT ordered solutions is high. For example, it is much higher than that reported for ordered solutions of poly(γ-benzyl glutamate) (PBG), poly(γ-benzyl L-glutamate) (PBLG), or tobacco mosaic virus (TMV) at similar concentrations, e.g., for $\Phi/\Phi^* < 2.5$, $\lvert n_e - n_o \rvert \leq 5 \times 10^{-3}$ for both TMV and PBLG for example.[13-16] These smaller values for PBLG, TMV, etc., may be attributed in part to the helocoidal structure of these molecules. The normalized birefringence for pure PBT material $\lvert n_e - n_o \rvert/\phi$ obtained here are, however, higher than $\lvert n_e - n_o \rvert$ for some conventional thermotropic liquid crystals such as PAA or MBBA for example, where $\lvert n_e - n_o \rvert$ reaches values about 0.3–0.4 for the latter for temperatures far from the clearing point; a weaker order parameter characterizes these media: $S \simeq 0.5$–0.6.[33,42-47]

Conclusion

The results reported above exhibit an unexpected insensitivity of the order parameter S on the volume fraction ϕ of the rodlike solute PBT over the range $1.1 < \phi/\phi^* < 2.5$. Furthermore, S is deduced to be surprisingly close to unity over the entire concentration range studied. Here, S is deduced from the dependence of the birefringence $\lvert n_e - n_o \rvert$ on ϕ and therefore requires a number of assumptions discussed in the preceding sections. It would be desirable to confirm the conclusions reached here on the variation of S with ϕ using an independent technique, e.g., measurement of the diamagnetic susceptibility. A possible reason for the unexpected behavior may be related to the way in which the aligned solutions were formed, making use of an aligning magnetic field on a nematic solution confined between parallel plates. Studies are in progress to assess whether S might be increased from its normal equilibrium value for the bulk nematic PBT solution under such conditions. If not, it will be of interest to consider whether other special factors might contribute to the observed behavior for $\lvert n_e - n_o \rvert$ and the deduced

behavior for S. Candidate factors would include the effects of electrostatic interactions among the protonated PBT solute chains.

The dispersion of the birefringence $|n_e - n_o|$ over the spectral range studied (514.5–1907 nm) is not considered to be abnormal but is due to the different dispersions of the ordinary and extraordinary refractive indices. Thus, although both can be fitted by the same expression over the range studied, one of the two adjustable parameters in that expression differs for n_e and n_o. These parameters lie in the range normally experienced with organic molecules in both cases. Measurements in the visible spectral range show that nematic solutions are strongly dichroic, with light polarized along the extraordinary axis being more strongly absorbed than that polarized along the ordinary axis.[12] Nevertheless, naive interpretation of the parameters used to fit the dispersion data suggests a larger extinction coefficient for light polarized along the ordinary axis for wavelengths in the ultraviolet range. Owing to the magnitude of the extinction coefficient for the latter wavelengths and the thickness of the samples, no direct information is available as yet on the dichroism in the ultraviolet for nematic solutions of PBT.

Although not novel in concept,[48] we are unaware of previous reports in which the procedures used here to measure n_e and n_o over a wide range of wavelengths have been so implemented.

Acknowledgment. We thank the Air Force of Scientific Research, AFOSR, for partial support and Professor R. B. Meyer for the helpful suggestions concerning conoscopy. We also benefited from fruitful discussions with Professor G. D. Patterson.

References and Notes

(1) de Gennes, P.-G. *The Physics of Liquid Crystals*; Clarendon Press: Oxford, U.K. 1974.
(2) Stephen, M. J.; Straley, J. P. *Rev. Mod. Phys.* **1974**, *46*, 617.
(3) Chandrasekhar, S. *Liquid Crystals*; Cambridge University Press: Cambridge, U.K., 1977.
(4) De Jeu, W. H. *Physical Properties of Liquid Crystalline Materials*; Gorden and Breach Science Publishers: New York, 1980.
(5) Mattoussi, H.; Berry, G. C. *Polym. Prep. (Am. Chem. Soc., Div. Polym. Sci.)* **1991**, *32* (3), 690.
(6) Lee, C. C.; Chu, S. G.; Berry, G. C. *J. Polym. Sci., Polym. Phys. Ed.* **1983**, *21*, 1573.
(7) Metzger Cotts, P.; Berry, G. C. *J. Polym. Sci., Polym. Phys. Ed.* **1983**, *21*, 1255.
(8) Furukawa, R.; Berry, G. C. *Pure Appl. Chem.* **1985**, *57*, 913 and references therein.
(9) Venkatraman, S. Ph.D. Dissertation, Carnegie Mellon University, Pittsburgh, PA, 1981.
(10) Tsai, H.-H. Ph.D. Dissertation, Carnegie Mellon University, Pittsburgh, PA, 1983.
(11) Sullivan, V. Ph.D. Dissertation, Carnegie Mellon University, Pittsburgh, PA, 1990.
(12) Srinivasarao, M. Ph.D. Dissertation, Carnegie Mellon University, Pittsburgh, PA, 1990.
(13) Murthy, N. S.; Knox, J. R.; Samulski, E. T. *J. Chem. Phys.* **1976**, *65*, 4835.
(14) Oldenbourg, R.; Wen, X.; Meyer, R. B.; Caspar, D. L. D. *Phys. Rev. Lett.* **1988**, *61*, 1851.
(15) Leadbetter, A. J. In *The Molecular Physics of Liquid Crystals*; Luckhurst, G. R., Gray, G. W., Eds.; Academic Press: New York, 1979.
(16) Dupre, D. P.; Lin, F. M. *Mol. Cryst. Liq. Cryst.* **1981**, *75*, 217.
(17) Rao, D. N.; Swiatkiecz, J.; Chopra, P.; Ghoshal, S. K.; Prasad, P. N. *Appl. Phys. Lett.* **1986**, *48*, 1187.
(18) Wei-Berk, C.; Berry, G. C. *J. Polym. Sci., Polym. Phys. Ed.*, in press.
(19) Kurtz, S. K. In *Quantum Electronics*; Rabin, H., Tang, C. L., Eds.; Academic Press: New York, 1975; Vol. 1, Part A, Chapter 3.
(20) Shen, Y. R. *The Principles of Nonlinear Optics*; Wiley: New York, 1984.
(21) Yariv, A. *Optical Electronics*, 3rd ed.; Holt, Rinehart and Winston: New York, 1985.
(22) *Oeuvres Completes d'Auguste Fresnel*; De Senarmont, H., Verdet, E., Fresnel, L., Publishers; Imprimerie Imperiale: Paris, 1866; Vol. 1.
(23) Born, M.; Wolfe, E. *Principles of Optics*, 6th ed.; Pergamon Press: Oxford, U.K., 1980.
(24) Bruhat, G. *Optique*, 6th ed.; Masson & Cie Editeurs: Paris, 1965.
(25) Cladis, P. E. *Phys. Rev. Lett.* **1972**, *28*, 1629.
(26) Kajzar, F.; Messier, J. *Phys. Rev. A* **1985**, *32*, 2353.
(27) *Nonlinear Optical Properties of Organic Molecules and Crystals*; Chemla, D. S., Zyss, J., Eds.; Academic Press: New York, 1987; Vols. 1 and 2.
(28) Demus, D.; Richter, L. *Texture of Liquid Crystals*; Springer-Verlag: Leipzig, 1978; and ref 1.
(29) Don Bloss, F. *An Introduction to Methods of Optical Crystallography*; Holt, Rinehart and Winston: New York, 1961.
(30) Ditchburn, R. W. *Light*; Interscience Publishers: New York, 1963.
(31) McCrone, W. H.; McCrone, L. B.; Delly, J. G. *Polarized Light Microscopy*; McCrone Research Institute: Chicago, 1987.
(32) Wolfe, W. L. In *Handbook of Optics*; Optical Society of America; Driscoll, W. G., Vaughan, W., Eds.; McGraw-Hill: New York, 1978; Section 7.
(33) Kuczynski, W.; Stryta, B. *Mol. Cryst. Liq. Cryst.* **1975**, *31*, 267.
(34) Kauzmanm, W. *Quantum Chemistry. An Introduction*; Academic Press: New York, 1957; Chapter 15.
(35) Mattoussi, H.; Berry, G. C., to be submitted for publication.
(36) Chang, R. *Mol. Cryst. Liq. Cryst.* **1975**, *30*, 155.
(37) (a) Chatelain, P. *Bull. Soc. Fr. Mineral.* **1937**, *50*, 280; **1955**, *78*, 262. (b) Chandrasekhar, S.; Krishnamurti, D.; Madhusudana, N. V. *Mol. Cryst. Liq. Cryst.* **1969**, *8*, 45.
(38) Vuks, M. F. *Opt. Spectrosc.* **1964**, *20*, 361.
(39) Tvetskov, V. N.; Eskin, V. E.; Frenkel, S. Y. *Structure of Macromolecules in Solutions*; English Translation; National Lending Library for Science and Technology: Boston, 1971; Vol. 1.
(40) Onsager, L. *Ann. N.Y. Acad. Sci.* **1949**, *51*, 627.
(41) Flory, P. J.; Ronca, G. *Mol. Cryst. Liq. Cryst.* **1979**, *54*, 289 and 311 and references therein.
(42) Chatelain, P.; Germain, M. *C. R. Acad. Sci., Paris* **1964**, *259*, 127.
(43) Chandrasekhar, S.; Madhusudana, N. V. *J. Phys. (Paris)* **1969**, *30*, 24.
(44) Brunet-Germain, M. *C. R. Acad. Sci., Paris* **1970**, *B271*, 1075; *Mol. Cryst. Liq. Cryst.* **1970**, *11*, 289 and references therein.
(45) Balzarini, D. A. *Phys. Rev. Lett.* **1970**, *25*, 914.
(46) Hanson, E. G.; Shen, Y. R. *Mol. Cryst. Liq. Cryst.* **1976**, *36*, 193.
(47) Laurent, M.; Journeaux, R. *Mol. Cryst. Liq. Cryst.* **1976**, *36*, 171.
(48) Kerkoc, P.; Zgonik, M.; Sutter, K.; Bosshard, C.; Gunter, P. *J. Opt. Soc. Am.* **1990**, *B7*, 313.

Registry No. PBT (SRU), 69794-31-6.